EXHIBIT B

TO DECLARATION OF SCOTT D. TANNER, PHD.

U.S. Patent Application Ser. No. 10/614,115

Inductively Coupled Argon Plasma as an Ion Source for Mass Spectrometric Determination of Trace Elements

Robert S. Houk, Velmer A. Fassel,* Gerald D. Flesch, and Harry J. Svec

Ames Laboratory—USDOE and Department of Chemistry, Iowa State University, Ames, Iowa 50011

Alan L. Gray

Department of Chemistry, University of Surrey, Guildford, Surrey, England GU2 5XH

Charles E. Taylor

Southeast Environmental Research Laboratory—USEPA, Athens, Georgia 30601

Solution aerosols are injected into an inductively coupled argon plasma (ICP) to generate a relatively high number density of positive ions derived from elemental constituents. A small fraction of these ions is extracted through a sampling orifice into a differentially pumped vacuum system housing an ion lens and quadrupole mass spectrometer. The positive ion mass spectrum obtained during nebulization of a typical solvent (1% HNO_3 in H_2O) consists mainly of ArH^+, Ar^+, H_3O^+, H_2O^+, NO^+, O_2^+, HO^+, Ar_2^+, Ar_2H^+, and Ar^{2+}. The mass spectra of the trace elements studied consist principally of singly charged monatomic (M^+) or oxide (MO^+) ions in the correct relative isotopic abundances. Analytical calibration curves obtained in an integration mode show a working range covering nearly 4 orders of magnitude with detection limits of 0.002–0.06 μg/mL for those elements studied. This approach offers a direct means of performing trace elemental and isotopic determinations on solutions by mass spectrometry.

Despite the demonstrated utility of mass spectrometry for the analysis of a wide variety of gaseous or solid samples, this technique is scarcely used for the routine determination of elemental constituents in aqueous solutions. Commonly used ion sources are not suitable for the rapid, direct examination of aqueous samples because extensive sample preparation procedures are required (*1*, *2*). Thus, the sample is evaporated onto a filament for thermal ionization or incorporated into an electrode for spark ionization before the sample-containing substrate is physically mounted in the vacuum system. The associated time requirement for these operations renders the routine analysis of large numbers of solutions impractical.

Elemental constituents in solution samples are commonly determined by atomic absorption or emission spectrometry. In these techniques solution aerosols are injected directly into a variety of high-temperature atomization cells at atmospheric pressure for vaporization, atomization, and excitation. These flames and plasmas often provide significant populations of positive ions, which can be extracted through an appropriate sampling orifice into a vacuum system for mass analysis and detection (*3–20*). Ions derived from elemental constituents of injected solution aerosols should also be extractable by a similar approach. Thus the analytical capabilities of mass spectrometry can, in principle, be combined with the convenience and efficiency of solution introduction into an appropriate plasma ion source.

A.L.G. has previously evaluated a system for trace element determinations based on the introduction of solution aerosols into a dc capillary arc plasma (CAP) (*21*). A small fraction of plasma gas along with its ions was extracted from the CAP through a pinhole-like sampling orifice into a differentially pumped vacuum system containing an electrostatic ion lens, quadrupole mass analyzer, and electron multiplier. Background mass spectra obtained from the CAP had few peaks above 50 amu and thus facilitated use of a low-resolution mass analyzer. Analyte elements were detected essentially as singly charged, monatomic, positive ions, i.e., the simplest possible mass spectrum. Detection limits of 0.000 02–0.1 μg/mL were obtained; those elements with ionization energies below 9 eV had the best powers of detection (*22–24*). The relative abundances of the various isotopes of Sr and Pb were determined with relative precisions of ±0.5% in dissolved mineral samples (*25*, *26*). These results indicated the feasibility of obtaining elemental mass spectra from analytes in solution with a plasma ion source. However, matrix and interelement interferences were severe (*26*).

Although both the CAP and the inductively coupled plasma (ICP) were originally developed for trace element determinations by atomic emission spectrometry, the ICP has found much wider application. Most of the characteristics of the ICP that have vaulted it to supremacy as an excitation source for atomic emission spectrometry are also highly desirable in an ion source for mass spectrometry (*27–29*). In particular, a high number density of trace element ions is implied by the common use of emission lines from excited ions for the determination of trace elements by atomic emission spectrometry. For example, cadmium, despite its relatively high ionization energy (8.99 eV), is often determined by using an ion line (*30*). Also, the ICP as an excitation source is remarkably free from such interferences as (a) incomplete solute vaporization and atomization and (b) ionization suppression or enhancement caused by changes in the solution concentration of easily ionized concomitant elements, e.g., Na (*31–34*). The objective of the present work is to present results that demonstrate the feasibility of inductively coupled plasma–mass spectrometry (ICP-MS) for the determination of elemental concentrations and isotopic abundance ratios in solutions.

APPARATUS AND PROCEDURES

The ICP-MS apparatus used in the present work is shown schematically in Figure 1. The components and operating conditions are listed in Table I. The apparatus has been described in greater detail elsewhere (*35*).

Inductively Coupled Plasma. The ICP was generated in a horizontal torch fitted with an extended outer tube as shown in Figure 1. The tube extension merely elongated the ICP relative to its dimensions in torches of conventional length. As viewed from its end, the extended ICP had the usual toroidal appearance. Thus, the injected aerosol particles remained localized in the central or axial channel of the ICP, where vaporization, atomi-

0003-2700/80/0352-2283$01.00/0

Table I. Instrumental Facilities

Component description manufacturer	Operating conditions	Component description manufacturer	Operating conditions
Plasma generator: Type HFP-2500D with impedance matching network. Plasma-Therm, Inc. Kresson, NJ	Forward power 1000 W, reflected power <10 W, 27.12 MHz	Ion lens voltage supply: Model 275-L25. Extranuclear Laboratories, Inc. Pittsburgh, PA	Operated in atmospheric pressure ionization mode (electron impact ionizer off)
Plasma torch: all quartz. Ames Laborabory design and construction (*29*) with outer tube extended 50 mm above tip of aerosol tube	Argon flow rates: plasma flow 12 L/min aerosol carrier flow 1 L/min auxillary flow used only during ignition	Quadrupole mass spectrometer: Model 100C. Uthe Technologies, Inc. (UTI) Sunnyvale, CA	Minor modifications described in text
Ultrasonic nebulizer: Model UNS-1. Plasma Therm, Inc. Kresson, NJ. similar to Ames Laboratory design (*36*). modified Margoshes-Veillon desolvation system (*37*)	Sample introduction rate 2.5 mL/min by peristaltic pump, transducer power ~50 W, transducer and condenser ice water cooled	Detector: Channeltron electron multiplier Model 4717. Galileo Electro-Optics Corp. Sturbridge, MA. Supplied by UTI	Cathode bias −4 kV, gain ≈ 10^6, anode electrically isolated from channel
Orifice disk: molybdenum disk. Agar Aids. Stansted, Essex, England	Two mm o.d. 0.5 mm nominal thickness, orifice length ≈ orifice diameter, 50 μm orifice diameter	Pulse counting system: Model 1121 preamplifier-discriminator Model 1109 counter. EG&G Princeton Applied Research. Princeton, NJ	Single discriminator mode, threshold 3 mV
Vacuum system: welded stainless steel assembly, differentially pumped. Ames Laboratory construction	First stage pressure: 1 × 10^{-3} torr (air, 1 atm, 25 °C), 4 × 10^{-4} torr (ICP sampling); second stage pressure: 1 × 10^{-4} torr (ICP sampling)	Data acquisition (scanning mode): active low pass filter-amplifier Model 1020. Spectrum Scientific Corp. Newark, NJ	Spectrum recorded on X-Y recorder: *Y* axis, filtered and amplified dc voltage (proportional to count rate from counter); *X* axis, dc voltage (0 to +10 V) from mass spectrometer controller (proportional to transmitted mass)
Ion lens elements: stainless steel, based on Model 275-N2. Extranuclear Laboratories, Inc. Pittsburgh, PA	Voltage values: $V_1 = -200$ V, $V_2 = -80$, $V_3 = -95$, $V_4 = -60$, $V_{DP} = -60$, $V_{FOCUS} = -18$, $V_{RODS} = -11$	Data acquisition and handling (integration mode): Counter interfaced to teletype for paper tape, hard copy record	Mass spectrometer manually peaked on mass of interest, count period 10 s, 5-10 count periods recorded and averaged at each mass and for each solution

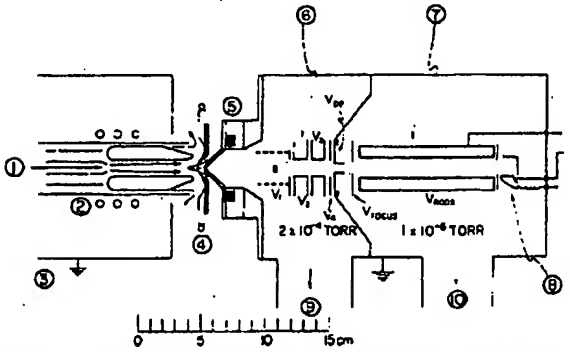

Figure 1. Schematic diagram of ICP, ion sampling interface, and vacuum system: (1) analyte aerosol from nebulizer; (2) ICP torch and load coil; (3) shielding box; (4) skimmer with plasma plume shown streaming through central hole; (5) sampler cone with extraction orifice (detailed diagram in Figure 2); (6) electrostatic ion lens assembly; (7) quadrupole mass analyzer; (8) channeltron electron multiplier; (9) pumping port to slide valve and diffusion pump (first pumping stage); (10) pumping port to slide valve, liquid nitrogen baffle, and diffusion pump (second pumping stage).

zation, and ionization of analyte species occurred as in conventional ICPs (*27-29*). The torch was enclosed in a grounded, copper-lined shielding box.

Plasma Sampling Interface. The function of the interface was to extract a small fraction of plasma gas, along with its ions,

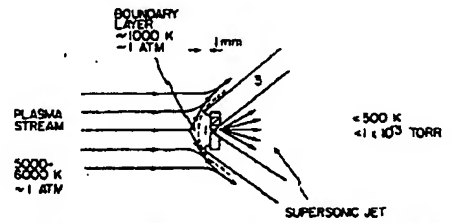

Figure 2. Cross-sectional diagram of sampler tip: (1) sampling orifice (50 μm diameter); (2) molybdenum disk containing orifice; (3) copper cone with spun copper seal to retain molybdenum disk.

into the vacuum system. The extraction was performed in two steps with the skimmer and sampler shown in Figure 1. The axial channel region of the ICP flowed through the central hole of the water-cooled, stainless steel skimmer, forming a well-defined plume. Analyte species derived from the sample aerosol streamed through the skimmer hole with the plume, while the outer portions of the vortex of the ICP were deflected outside the skimmer. The plume, still near atmospheric pressure, next impinged on the sampler, which consisted of a water-cooled copper cone mounted on the vacuum system. Plume particles (atoms, ions, and electrons) were extracted through a 50 μm diameter orifice drilled through the center of a molybdenum disk. The disk was mounted in the tip of the sampler behind a retaining copper lip as shown in Figure 2. The copper lip held the disk firmly in position, served as a vacuum seal, and provided thermal contact between the disk and the cooled sampler cone.

The stainless steel skimmer glowed orange hot (~1000 K) when immersed in the ICP. The tip of the sampler glowed red hot (~800 K) when thrust inside the skimmer. These elevated temperatures greatly inhibited the condensation of analyte-derived solids on either the skimmer or sampler tip. When such condensation became extensive, ion sampling was unstable, i.e., solid deposits plugged the sampling orifice or the ICP arced sporadically to the skimmer and sampler. Maximum count rates for analyte ions were obtained when the sampler tip was thrust inside the skimmer about 2 mm behind the skimmer tip.

A typical sampler operated in a stable fashion for nebulization of dilute (<150 μg/mL) analyte solutions for 8–10 h before sampling conditions deteriorated due to gradual condensation of solid on the tip of the sampler. The sampler was readily cleaned by immersing it in an ultrasonically agitated water bath for a few minutes. An individual sampler remained useful for a total of 50–100 h. During this time the disk gradually became pitted and discolored, and the orifice developed an irregular cross section.

A Teflon gasket and nylon bolts were used to retain the cooling flange and to isolate it electrically from the vacuum system. The skimmer and sampler were each grounded through separate inductive–capacitive filters (*36*). This grounding scheme reduced RF interference in the ion gauges, counting electronics, and recording equipment.

Vacuum System. The sampler cone and orifice assembly were mounted on a two-stage, differentially pumped vacuum system of welded stainless steel construction. The first stage was evacuated by an oil diffusion pump (1600 L s^{-1}, Lexington Vacuum Division, Varian Associates, Lexington, MD). The electrostatic ion lens was mounted in the first stage. As shown in Table I, the first-stage pressure was sufficiently low for ion collection and beam formation but too high for mass spectrometer operation. A second stage of differential pumping was therefore required. The ions were directed through a 3 mm diameter × 8 mm long aperture into the second stage, which housed the quadrupole mass spectrometer. The second stage was pumped by a second 1600 L s^{-1} oil diffusion pump equipped with a liquid nitrogen cooled baffle. Both pumping stations were provided with slide valves to permit rapid venting for sampler installation or modification of internal components.

Electrostatic Ion Lens System. An ion lens system was used to collect positive ions from the supersonic jet of sampled gas while neutral particles were pumped away. The ions were then focused and transmitted to the mass analyzer. As shown in Figure 1, the lens system consisted of a set of coaxial, sequential cylinders, each biased at a particular dc voltage. Maximum ion signals were obtained at the voltages specified in Table I (*35*). The shapes, width, resolution, and symmetry of the ion peaks were unaffected by the voltage settings on the ion optical elements. The cylindrical section of the first element was made of no. 16 mesh screen to provide fast pumping of neutral species from the ion collection and collimation region. A 4.6 mm diameter solid metal disk was positioned in the center of the first element. This disk acted as an optical baffle, i.e., it blocked the line of sight from the ICP through the sampling orifice, lens system, and quadrupole axis, and thus helped to prevent optical radiation from the ICP from reaching the electron multiplier.

Mass Analyzer. The quadrupole mass analyzer (originally supplied as a residual gas analyzer) was modified as follows. First, the filaments, grid, and reflector of the electron impact ionizer were removed; the focus plate was retained as the quadrupole entrance aperture. The latter was aligned visually with the center of the lens system by shimming under the rod mounting bracket. Second, the rods were biased below ground by connecting separate dc supplies into the dc rod driver circuit. The mass analyzer had a mass range of 1–300 amu with resolution sufficient to resolve adjacent masses unless one peak was much more intense than the adjacent one. Because the transmission of the mass analyzer dropped significantly as the transmitted mass increased, the observation of relatively low analyte masses was emphasized in this feasibility study.

Electron Multiplier and Pulse Counting Electronics. The Channeltron electron multiplier detector as supplied with the mass analyzer was operated in the pulse counting mode. Although this multiplier had a much lower gain than those designed specifically for pulse counting, it still performed adequately for the following reasons. First, there was no evidence of loss of gain or pulse overlap at count rates up to at least 5×10^4 counts/s. The multiplier therefore had a linear dynamic range of at least 5×10^4. At −4 kV the threshold setting on the pulse counting equipment could be set over a broad range (0.2–30 mV) without attenuating the observed count rate. The pulses were conducted from the multiplier anode to a preamplifier–discriminator–counter system. The counting threshold was set just above the height of RF noise pulses from the ICP.

Mass Spectra, Analytical Calibration Curves, and Detection Limits. The reference blank solution and the matrix for the reference solutions used for calibration consisted of 1% (volume) nitric acid, prepared by diluting doubly distilled, concentrated nitric acid with deionized water. The reference calibration solutions were prepared by appropriate dilution of stock solutions. The stock solutions were prepared by dissolving pure metals or reagent grade salts in dilute nitric acid.

Mass spectra were acquired in the scanning mode as described in Table I. Individual points for analytical calibration curves were obtained in the integration mode. The average total count for the reference blank solution at the mass of interest was evaluated first, followed by the average total count for each reference calibration solution, in ascending order of concentration. The average total count for the reference blank was then subtracted from the average total count for each reference standard solution before plotting. The detection limit was calculated as the analyte concentration required to give an average net count equal to twice the standard deviation observed at the mass of interest for the blank solution, $2\sigma_b$.

RESULTS AND DISCUSSION

Boundary Layer Formation. As the flowing plasma plume approached the sampler, the plume gas was deflected around the blunt sampler tip. As shown in Figure 2, an aerodynamically stagnant layer of gas formed between the flowing plume and the sampler tip (*10, 15, 16, 38–40*). Formation of a space–charge sheath or electrical double layer in contact with the sampler was also probable (*40–44*). This composite boundary layer was in thermal contact with the relatively cool sampler. Thus, the temperatures in the boundary layer were intermediate between the plume and sampler temperatures. The boundary layer extended across the sampler tip and was visibly unbroken by the gas flow drawn into the sampling orifice. Ion extraction into the vacuum system therefore occurred only after transport through the boundary layer, which would take 1–2 ms and involve up to ~10^6 collisions (*35*).

Such collisions in a medium temperature environment probably facilitated ion–electron recombination, ion neutralization at the sampler walls, charge exchange, ion–neutral attachment, nucleation and condensation of solid deposits, or other reactions (*10, 16, 38*). The metal surface of the orifice disk may have catalyzed some of these reactions occurring in the boundary layer or just inside the channel-like orifice (*15*). Also, collisions leading to clustering, ion–electron recombination, or charge exchange occurred in the supersonically expanding jet of extracted gas (*10, 11*). The effects of these reactions are described below.

Mass Spectra of Reference Solutions. The mass spectrum of the major positive ions from the ICP plume observed during nebulization of a reference blank solution is shown in Figure 3. The two most intense peaks corresponded to Ar^+ (40 amu) and ArH^+ (41 amu). A comparable peak for H^+ (1 amu) was evident, with its low mass edge obscured by "zero blast", i.e., ions anomalously transmitted through the quadrupole field region at the beginning of a scan because the low applied potentials led to very weak fields within the rod structure (*2*).

The major ions observed in the mass spectrum of the reference blank solution are identified in Table II. All of the major ions have been observed previously by other investigators in the mass spectra of flames and plasmas (*5, 17, 18,*

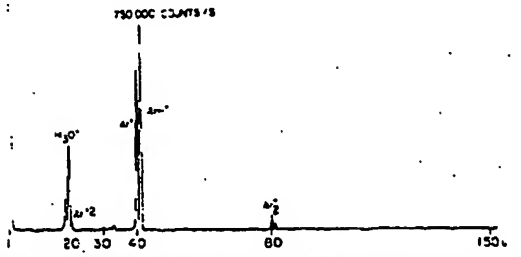

Figure 3. Positive ion mass spectrum of reference blank solution (1% HNO_3 in deionized distilled water). Vertical scale is linear with count rate; base peak count rate is indicated. The background ranged from 30 to 100 counts/s.

Table II. Major Ions Observed in Mass Spectrum of Reference Blank Solution

mass	ion(s)[a]	rel count rate[b] ArH^+ = 100	rel count rate[b] $^{55}Mn^+$ = 100
16	O^+	0.4	6
17	HO^+, NH_3^+	1	15
18	H_2O^+, NH_4^+	12	180
19	H_3O^+	40	600
20	Ar^{2+}	4	60
30	NO^+	4	60
32	O_2^+	2	30
33	$(O_2^+)\cdot H$	4	60
36	$^{36}Ar^+$	0.8	12
37	$^{36}ArH^+$ $(H_3O^+)\cdot H_2O$	1	15
40	$^{40}Ar^+$	75	1125
41	$^{40}ArH^+$ $(Na^+)\cdot H_2O$	100	1500
80	Ar_2^+	8	120
81	$(ArH^+)\cdot Ar$	3	45

[a] Possible ions at same mass number are listed in decreasing order of likelihood or probable intensity. [b] ArH^+ ≈ 750 000 counts/s; $^{55}Mn^+$ ≈ 50 000 counts/s at 50 μg/mL solution concentration.

20, 22, 23) or as analogous cluster species formed during supersonic jet expansions. Of the major ions only Ar^+ has been identified in analytical ICPs by optical spectrometry, and even that identification is tentative or disputed (30, 45). The existence of an intense peak due to ArH^+, along with the observation of other cluster ions such as H_3O^+ (19 amu) and Ar_2^+ (80 amu) indicated that some clustering reactions occurred during ion extraction. Some minor ions (≤1000 counts/s) were observed at times at 2, 45–48, 50, 54–59, 68–70, 73, and 76 amu. Many of these were also formed during the extraction process, e.g., $O_2^+\cdot H_2O$ at 50 amu. Despite the opportunities for complicating reactions described above, the mass spectrum of the reference blank solution had usefully clear mass regions from 2 to 13 amu, from 21 to 29 amu, and from 42 amu up.

Because there was no ion source inside the vacuum system, the residual gas was not ionized. Ions derived from pump oil were not observed. Thus, a major background contribution from ionization of residual gas in conventional ion sources was not observed with the plasma ion source (22, 23).

The count rate obtained for the reference blank spectrum at those masses free of major or minor ions was 30–100 counts/s, well above the dark current count rate characteristic of the electron multiplier (≤1 count/s). This background count rate was the same at all masses and was independent of the ion lens voltages and mass spectrometer operating conditions. Apparently, this background was caused by vacuum UV photons striking the electron multiplier. These

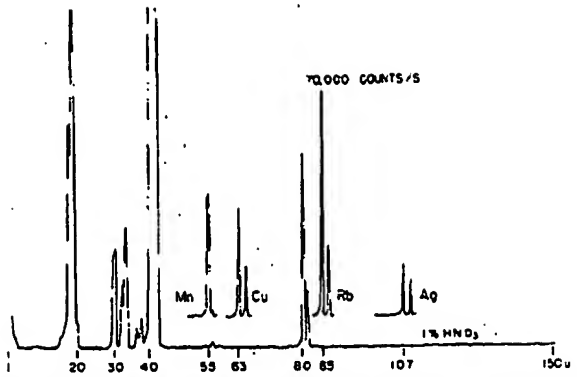

Figure 4. Reference blank spectrum (bottom); superimposed spectra are from 50 μg/mL solutions of the indicated element in 1% HNO_3. Vertical scale sensitivity is 10 times that of Figure 3.

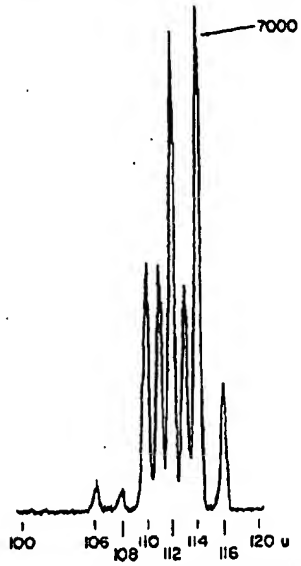

Figure 5. Mass spectrum of Cd at 50 μg/mL in 1% HNO_3.

photons probably were radiated directly from the ICP and also from the decay of metastable argon atoms within the vacuum system. Although the direct line-of-sight from the orifice through the quadrupole field region was blocked by a disklike baffle (Figure 1) and the multiplier was offset from the quadrupole axis, numerous photons still struck the multiplier. The background count rate (photons + minor ions, if present) at each mass of interest of the reference blank solution was reproducible during a 5–10-h period, and integration data for reference standards were adequately corrected by subtraction of the reference blank spectrum.

The recorded peaks of monatomic, singly charged positive ions from solutions of Mn, Cu, Rb, and Ag are shown superimposed on the reference blank spectrum in Figure 4. The metal ion spectra are plotted on the same mass and count rate scales as the reference blank spectrum but are displaced vertically by a change in the recorder zero. As shown in the figure, the accepted relative abundances of the isotopes of Cu, Rb, and Ag were observed. The mass spectrum of Cd is shown in Figure 5; again, the count rates for the various isotopes corresponded to the accepted relative isotopic abundances. The peaks were symmetrical and nearly triangular, as expected for quadrupole mass analysis of ions having a low kinetic energy spread. The least abundant Cd isotope ($^{106}Cd^+$, 0.88%) was clearly detected. For the elements shown in Figures 4

Table III. Relative Isotopic Abundance Determination of Naturally Occurring Copper Isotopes, 2.5 μg/mL Cu in 1% HNO,

				% abundance	
Isotope	N^a	σ	$N^{1/2}$	determined	accepted
$^{63}Cu^+$	19786	740	143	69.9 ± 1.1	69.1
$^{65}Cu^+$	8505	546	98	30.1 ± 1.1	30.9

[a] N = background subtracted average count, obtained in integration mode as described in Apparatus and Procedures section. Uncertainties are indicated at 95% confidence level for 15 determinations, counting time 10 s for each determination.

and 5, and for most of the elements studied, only monatomic, singly charged ions (M^+) were observed. Several elements were detected as a distribution of M^+ and MO^+ ions, e.g., Ti, As, and Y. The only doubly charged analyte ions observed were Ba^{2+} and Sr^{2+}, i.e., from the two elements with the lowest second ionization energies. Also, no Cu^+ or Mo^+ ions were observed from the orifice assembly. Thus, the mass spectra obtained were remarkably simple, which facilitated use of a low-resolution mass analyzer.

Isotopic Abundance Determinations. The utility of the ICP-MS approach for the direct determination of isotopic abundances of elemental constituents in solutions is illustrated further by the data shown in Table III. The agreement with the accepted values of the relative abundances of $^{63}Cu^+$ and $^{65}Cu^+$ was within the estimated uncertainty in the determined values. The absolute standard deviation of the count was approximately 5 times greater than the square root of the average count, which indicated that the uncertainty in the count was significantly greater than the uncertainty expected from counting statistics. This increased uncertainty was undoubtedly due to instability of some instrumental parameter; instability in nebulizer efficiency and ion extraction efficiency through the boundary layer were likely culprits. Thus the precision of the isotopic ratio determinations in Table III is expected to improve with continued development of the ICP-MS technique.

These isotope ratio determinations were performed directly on a trace level of copper in solution. Also, the total time for the determination of both isotopes was 5 min, including the time required for sample interchange, nebulizer equilibration, and adjustment of the mass transmitted by the mass analyzer. Thus, 100 isotopic ratio determinations could easily be performed in a single day, indicating the potential of the ICP-MS approach for rapid isotopic abundance determinations of trace levels of elements in large numbers of solutions.

Analytical Calibration Curves and Detection Limits. The analytical calibration curves shown in Figure 6 which were obtained in the integration mode, show a useful working range of 3 to 4 orders of magnitude. These data were obtained from reference solutions containing only one element.

When the plasma plume was first moved into contact with the sampler, the count rates of all the ions increased rapidly. After about 1 h this rate of increase tapered off so that the calibration data could be obtained. The Co and Mn curves in Figure 6 show replicate determinations at the 0.02 μg/mL level. For Co and Mn the point labeled by the arrow was determined first. The unlabeled points at 0.02 μg/mL were determined after the calibration data at higher concentrations were obtained, i.e., after about 30 min. This small positive deviation was not caused by memory; instead it reflected the general tendency of the count rates of all the ions to increase slowly with time (~20% every hour) in the absence of orifice plugging. This gradual increase was not accompanied by any discernible increase in orifice diameter. Some subtle phenomena related to the plasma sampling process apparently caused the number of extracted ions to increase with time. This increase should not affect isotope ratio measurements provided they are performed by rapid, repetitive scanning or peak switching techniques. For determination of elemental concentrations, normalization of the ion count rate to an internal standard ion or to a total beam monitor signal should provide internal compensation for the increasing ion signals.

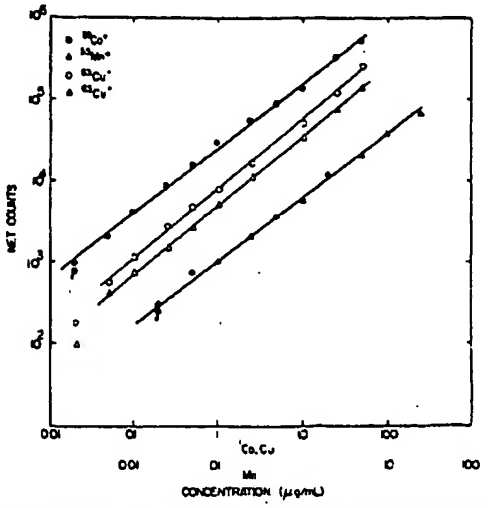

Figure 6. Analytical calibration curves obtained in integration mode. Read bottom scale for Mn curve.

Table IV. Detection Limits Obtained

element	ion detected	% abundance	detection limit ($2\sigma_b$) μg/mL	ppma[a]
Mg	$^{24}Mg^+$	78.6	0.006	0.004
Cr	$^{52}Cr^+$	83.8	0.002	0.0007
	$^{53}Cr^+$	9.6	0.01	0.003
Mn	$^{55}Mn^+$	100	0.003	0.001
Co	$^{59}Co^+$	100	0.006	0.002
Cu	$^{63}Cu^+$	69.1	0.009	0.002
	$^{65}Cu^+$	30.9	0.02	0.005
Rb	$^{85}Rb^+$	72.2	0.008	0.002
	$^{87}Rb^+$	27.8	0.02	0.004
As	$^{75}AsO^+$	100 (^{75}As)	0.06	0.01
Y	$^{89}YO^+$	100 (^{89}Y)	0.04	0.008

[a] ppma = DL(μg/mL) × (18/(atomic weight)).

The detection limits obtained for selected elements are listed in Table IV. The detection limits for the major isotopes of Cr, Cu, and Rb were lower than those for the corresponding minor isotopes by factors approximately equal to the relative isotopic abundances. Because the reference blank spectrum had minor peaks (<1000 counts/s) at 54, 56, and 59 amu, the standard deviation of the reference blank count rate increased in the order 52 amu (photons) < 55 amu (photons + ions from peak edges at 54 and 56 amu) < 59 amu (photons + minor ions). Thus the detection limits were degraded in the same order, i.e., $^{52}Cr^+ < {}^{55}Mn^+ < {}^{59}Co^+$, although the net counts at these masses were similar for equimolar solutions of these three elements. It is clearly desirable to reduce both the number and count rates of minor ions in the reference blank spectrum and the count rate of the photon background.

The detection limits listed in Table IV were obtained with a sampler that provided more AsO^+ and YO^+ than As^+ and Y^+ ions; hence the oxide ions were used for the determinations of the detection limits of these two elements. Useful analytical calibration curves for As and Y were obtained up to at least

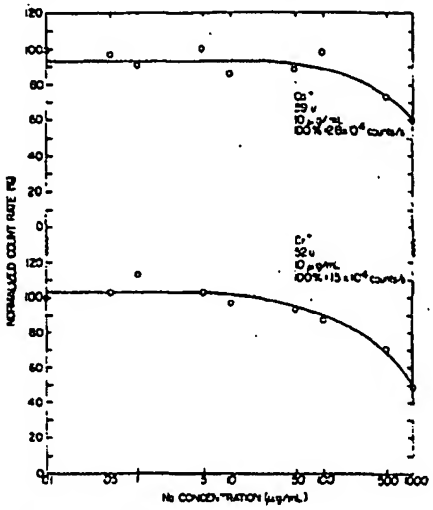

Figure 7. Effect of Na concomitant concentration on count rates of $^{52}Cr^+$ and $^{59}Co^+$, integration mode, 10 s count time, ~5 count periods averaged for each point.

50 μg/mL for either the metal or metal oxide ion. Although formation of metal oxide ions was not desirable, these ions were still useful analytically. Also, metal oxide ion formation is not expected to cause serious mass spectral interferences, because most of the elements are not detected as oxide ions, and the masses and isotopic distribution of MO^+ ions are predictable for those elements with a high probability of oxide formation.

The ICP-MS detection limits in Table IV were poorer, i.e., larger numbers, than the CAP-MS detection limits by factors of 10–100. This discrepancy is largely accounted for by the longer integration time (30 s), larger orifice diameter (75 μm), and much lower background levels and background standard deviations obtained in the CAP-MS study. Indeed, the standard deviation of the background in the CAP-MS study was so low (~1 count/s) that the conventional definition of detection limit was considered inappropriate (*22*, *23*). The CAP-MS detection limits were superior to those characteristic of all other techniques for trace elemental analysis. Unfortunately, these powers of detection were of little analytical value because of severe interelement interference effects (*26*).

The ICP-MS detection limits in Table IV represent potentially useful powers of detection, which can undoubtedly be enhanced by experimental improvements in ion extraction and transmission efficiency and optical baffling of the electron multiplier. Furthermore, the ICP-MS approach should be less susceptible to interelement interference effects than CAP-MS because of the superior sample injection, vaporization, and atomization capabilities and higher electron number density of the ICP (*27–29*, *32*). This expectation is partially demonstrated below.

Ionization Type Interelement Effects. As mentioned above, the ICP as an atomization–excitation source for atomic emission spectrometry is relatively free from ionization interferences caused by easily ionizable elements in solution. For example, the intensities of certain emission lines of excited ions of Ca, Cr, and Cd show little dependence on Na concentration from 0 to 7000 μg/mL (*32*, *33*). In the present work, the count rates of mass resolved analyte ions were suppressed to a somewhat greater extent in the presence of Na as shown in Figure 7. Each point plotted in this figure was normalized to a reference count rate for the same solution concentration of the analyte ion in the absence of Na. Because solute concentrations ≥150 μg/mL gradually clogged the orifice with condensed solid, the reference count rate gradually decreased and was therefore determined repeatedly. The arbitrary nature of this correction procedure, coupled with a significant long-term drift in aerosol intensity produced by the ultrasonic transducer, led to the scatter of the points shown in Figure 7. These plots exhibited a shape similar to those observed for atomic emission spectrometry by Larson et al. (*32*, *33*). Because of the ultrasonic nebulizer used in the present work, 1000 μg/mL Na corresponded roughly to 10000 μg/mL Na in Larson's work, which was performed with a pneumatic nebulizer (*36*).

The magnitude of suppression of analyte ionization shown in Figure 7 is approximately twice as large as that observed by atomic emission spectrometry by Larson et al. (*32*) if the latter data are adjusted for the approximately tenfold difference in nebulization efficiency. This difference may be rationalized as follows. In the present work, ion extraction occurs through an unbroken boundary layer that is somewhat cooler than the unperturbed plasma. Ion–electron recombination or electron loss to the sampler wall may occur at a significant rate in this layer, leading to an effective electron number density (n_e) in the vicinity of the orifice that is less than that prevalent in the unperturbed plasma. For this lower value of n_e, the "extra" electrons contributed by the ionization of Na should be more significant, causing a proportionately greater increase in the total n_e near the orifice. Thus, the greater suppression of analyte ionization observed in the present work may be a characteristic of the boundary layer rather than the unperturbed plasma. A strict comparison of the magnitudes of the ionization suppressions observed in the present work with those observed from the ICP by atomic emission spectrometry is therefore not necessarily valid.

To place the ionization type interelement effect measured in the present work into perspective, we note that the degree of suppression of analyte ionization was far less severe than that observed for the capillary arc plasma–mass spectrometric approach (*26*) or for flames and other plasmas that have been used as atomization sources in atomic emission or absorption spectrometry (*31*, *33*). Furthermore, the >100 μg/mL Na range, where ionization suppression was significant, represented the analytical equivalent of determining the Co and Cr content of NaCl. Thus, analytical calibrations established for the determination of Co and Cr in a deionized water matrix would have yielded analytical results only ~12% lower if the sample calibrations were used for the analysis of a NaCl sample prepared as a solution of approximately 100 μg/mL Na. Even only approximate matching of the total concentration of easily ionizable elements in reference calibration solutions and samples would essentially eliminate analytical bias caused by ionization type interferences, including samples in which these elements (e.g., Na or K) represent varying major fractions of the total metal content.

Solid Deposition in the Sampling Orifice. Solid condensation in or near the orifice remains an operational problem. As mentioned above, normalization of analyte ion count rates either to an internal standard ion or to a beam monitor signal should correct for the gradual decrease in extraction efficiency of analyte ions caused by progressive solid condensation expected from solutions such as hard water. However, progressive deposition of sample material does restrict the useful life of orifices exposed to solutions whose total solute concentrations are above approximately 150 μg/mL. Thus, biological fluids such as urine or blood serum would require a dilution factor of several hundred before analyses of such solutions could be performed for more than about 1 h. The consequent deterioration in powers of detection for analyte elements may not be acceptable for various applications.

Sample deposition in the orifice is primarily caused by the formation of involatile metal compounds in the relatively cool, stagnant gas of the boundary layer shown in Figure 2. Potential solutions to the troublesome deposition of sample material in the orifice undoubtedly lie in the geometry and operating conditions of the sampler tip, which govern boundary layer formation. For example, solid deposition should be less significant in orifices of diameter >50 μm, which would also extract more ions into the vacuum system. A more streamlined, conical orifice assembly should deflect the plasma stream smoothly around the cone tip, instead of allowing a stagnant layer of gas to build up outside the extraction orifice (Figure 2) (*10*, *11*, *15*, *16*, *38*, *40*). Such refinements are expected to relax the compromise between powers of detection, dilution factors, and orifice lifetimes, thus facilitating application of the ICP-MS approach to elemental and isotopic determinations in samples of total solute content greater than 150 μg/mL.

ACKNOWLEDGMENT

The contributions of Tom Johnson and Garry Wells of the Ames Laboratory machine shop are gratefully acknowledged.

LITERATURE CITED

(1) Ahearn, A. J., Ed. "Trace Analysis by Mass Spectrometry"; Academic Press: New York, 1972; Chapter 1.
(2) Dawson, P. H., Ed. "Quadrupole Mass Spectrometry and Its Applications"; Elsevier: New York, 1976; p 323.
(3) Drawin, H. W. In "Plasma Diagnostics"; Lochte-Holtgreven, W., Ed.; Wiley: New York, 1968; Chapter 13.
(4) Fristrom, R. M. *Int. J. Mass Spectrom. Ion Phys.* **1975**, *16*, 15–32.
(5) Goodings, J. M.; Bohme, D. K.; Ng, C. W. *Combust. Flame* **1979**, *36*, 27–43.
(6) Hasted, J. B. *Int. J. Mass Spectrom. Ion Phys.* **1975**, *16*, 3–14.
(7) Hastie, J. W. *Int. J. Mass Spectrom. Ion Phys.* **1975**, *16*, 89–100.
(8) Hayhurst, A. N.; Mitchell, F. R. G.; Telford, N. R. *Int. J. Mass Spectrom. Ion Phys.* **1971**, *7*, 177–187.
(9) Hayhurst, A. N.; Telford, N. R. *Combust. Flame* **1977**, *28*, 67–80.
(10) Hayhurst, A. N.; Kittelson, D. B.; Telford, N. R. *Combust. Flame* **1977**, *28*, 123–135, 137–143.
(11) Burdett, N. A.; Hayhurst, A. N. *Chem. Phys. Lett.* **1977**, *48*, 95–99; *Combust. Flame* **1979**, *34*, 119–134.
(12) Horning, E. C.; Horning, M. G.; Carroll, D. L.; Dzidic, J.; Stillwell, R. N. *Anal. Chem.* **1973**, *45*, 936–943; **1975**, *47*, 1308–1312, 2369–2373; **1976**, *48*, 1763–1768; *J. Chromatogr.* **1974**, *99*, 13–21.
(13) Knewstubb, P. F. "Mass Spectrometry and Ion-Molecule Reactions"; Cambridge University: London, 1969; Chapter 2.3.
(14) Milne, T. A.; Greene, F. T. *Adv. Chem. Ser.* **1966**, *No. 72*, Chapter 5.
(15) Morley, C. *Vacuum* **1974**, *24*, 581–584.
(16) Perlel, R. *Int. J. Mass Spectrom. Ion Phys.* **1975**, *16*, 39–52.
(17) Prokopenko, S. M. J.; Laframboise, J. G.; Goodings, J. M. *J. Phys. D* **1972**, *5*, 2152–2160; **1974**, *7*, 355–362, 563–568; **1975**, *8*, 135–140.
(18) Rowe, B. *Int. J. Mass Spectrom. Ion Phys.* **1975**, *16*, 209–223.
(19) Siegel, M. W.; Fite, W. L. *J. Phys. Chem.* **1976**, *80*, 2871–2881.
(20) Vasile, M. J.; Smolinsky, G. *Int. J. Mass Spectrom. Ion Phys.* **1973**, *12*, 139–146; **1975**, *18*, 179–192; **1976**, *21*, 263–277.
(21) Jones, J. L.; Dahlquist, R. L.; Hoyt, R. E. *Appl. Spectrosc.* **1971**, *25*, 628–635.
(22) Gray, A. L. *Proc. Soc. Anal. Chem.* **1974**, *11*, 182–183; *Anal. Chem.* **1975**, *47*, 600–601; *Analyst (London)* **1975**, *100*, 289–299.
(23) Gray, A. L. In "Dynamic Mass Spectrometry"; Price, D., Todd, J. F. J., Eds.; Heyden: London, 1975; Vol. 4, Chapter 10.
(24) Applied Research Laboratories, Ltd., British Patent 1 261 596, 1969; U.S. Patent 3 944 828, 1976.
(25) Anderson, F. J.; Gray, A. L. *Proc. Anal. Div. Chem. Soc.* **1976**, *13*, 284–287.
(26) Gray, A. L. In "Dynamic Mass Spectrometry"; Price, D., Todd, J. F. J., Eds.; Heyden: London, 1978; Vol. 5, Chapter 8.
(27) Barnes, R. M. *CRC Crit. Rev. Anal. Chem.* **1976**, *7*, 203–286.
(28) Fassel, V. A. *Science* **1978**, *202*, 183–191; *Anal. Chem.* **1979**, *51*, 1290A–1308A; *Pure Appl. Chem.* **1977**, *49*, 1533–1545.
(29) Fassel, V. A.; Kniseley, R. N. *Anal. Chem.* **1974**, *46*, 1110A–1120A, 1155A–1164A.
(30) Winge, R. K.; Peterson, V. J.; Fassel, V. A. *Appl. Spectrosc.* **1979**, *33*, 206–219.
(31) Rubeska, I.; Raine, T. C. In "Flame Emission and Atomic Absorption Spectrometry"; Dean, J. A., Rains, T. C., Eds.; Marcel Dekker: New York, 1969; Vol. 1, Chapters 11 and 12.
(32) Larson, G. F.; Fassel, V. A.; Scott, R. H.; Kniseley, R. N. *Anal. Chem.* **1975**, *47*, 238–243.
(33) Larson, G. F.; Fassel, V. A. *Anal. Chem.* **1976**, *48*, 1161–1166.
(34) Kalnicky, D. J.; Fassel, V. A.; Kniseley, R. N. *Appl. Spectrosc.* **1977**, *31*, 137–150.
(35) Houk, R. S. Ph.D. Dissertation, Iowa State University, Ames, Iowa, 1980; Report IS-T-989; U.S. Department of Energy, Washington, DC, 1980.
(36) Olson, K. W.; Haas, W. J., Jr.; Fassel, V. A. *Anal. Chem.* **1977**, *49*, 632–637.
(37) Vellon, C.; Margoshes, M. *Spectrochim. Acta, Part B* **1968**, *23B*, 553–555.
(38) Biordi, J. C.; Lazzara, C. P.; Papp, J. F. *Combust. Flame* **1974**, *23*, 73–82.
(39) Reed, T. B. *J. Appl. Phys.* **1963**, *34*, 2266–2269.
(40) Clements, R. M.; Smy, P. R. *Combust. Flame* **1977**, *29*, 33–41.
(41) Boyd, R. L. F. *Proc. Phys. Soc. London, Sect. B* **1951**, *64*, 795–804.
(42) Oliver, B. M.; Clements, R. M. *J. Phys. D* **1975**, *8*, 914–921.
(43) Smy, P. R. *Adv. Phys.* **1976**, *25*, 517–553.
(44) Böhme, D. K.; Goodings, J. M. *J. Appl. Phys.* **1966**, *37*, 382–386, 4261–4268.
(45) Robin, J. *Analusis* **1976**, *6*, 89–97; *ICP Inf. Newsl.* **1979**, *4*, 495–509.

RECEIVED for review November 12, 1979. Resubmitted June 19, 1980. Accepted August 19, 1980. Presented in part at the Federation of Analytical Chemistry and Spectroscopy Societies 6th Annual Meeting, Philadelphia, PA, Sept 1979, and at the Pittsburgh Conference on Analytical Chemistry and Applied Spectroscopy, Atlantic City, NJ, March 1980. This work was supported by the U.S. Environmental Protection Agency and was performed at the Ames Laboratory, U.S. Department of Energy, Contract No. W-7405-Eng-82, under Interagency Agreement EPA-IAG-D-X0147-1.